THE EUROPEAN
PHYSICAL JOURNAL C

CrossMark

Accreting fluids onto regular black holes via Hamiltonian approach

Abdul Jawad[1,a], **M. Umair Shahzad**[1,2,b]

[1] Department of Mathematics, COMSATS Institute of Information Technology, Lahore 54000, Pakistan
[2] CAMS, UCP Business School, University of Central Punjab, Lahore, Pakistan

Abstract We investigate the accretion of test fluids onto regular black holes such as Kehagias–Sfetsos black holes and regular black holes with Dagum distribution function. We analyze the accretion process when different test fluids are falling onto these regular black holes. The accreting fluid is being classified through the equation of state according to the features of regular black holes. The behavior of fluid flow and the existence of sonic points is being checked for these regular black holes. It is noted that the three-velocity depends on critical points and the equation of state parameter on phase space.

1 Introduction

A very interesting physical phenomenon in astrophysics is the accretion of fluids onto a black hole (BH), which has been intensely discussed in the literature. The presence of an event horizon is a distinctive feature of a BH, which act as one way membrane through which accreting fluid or gas disappears and leads to several important issues. For instance, radiation emitted near the BH undergoes the effect of strong gravitational lensing and appears as the image of BH's shadow surrounded by sharp light ring. However, no inner boundary conditions are necessary for the equation of motion in the case of BH accretion [1]. On the other hand, one of the major challenges in general relativity is the existence of essential singularities and it looks like a common property in most solutions of the Einstein field equations.

Moreover, regular black holes (RBHs) have been constructed to resolve this problem because their metrics are regular everywhere and hence essential singularities can be avoided in the solutions of the Einstein equations of BHs physics [2]. These RBHs satisfied the weak energy condi-

tion while some of them violate the strong energy conditions [3,4]. However, the Penrose cosmic censorship conjecture suggests that singularities predicted by general relativity occur and they must be enclosed by an event horizon [5,6]. In this way, Bardeen [7] has done pioneering work and obtained a BH solution without any essential singularity at the origin enclosed by an event horizon known as a 'Bardeen black hole,' satisfying the weak energy condition. Later, many authors found similar solutions [8–10]. The coupling of general relativity to nonlinear electromagnetic theory has brought about new sets of charged RBHs. Hayward [11] and Berej et al. [12] found different kinds of RBH solutions. Recently, Leonardo et al. [13] used various distribution functions (such as the logistic, Fermi–Dirac, Dagum functions) in order to obtain charged RBHs. Kehagias–Sftesos (KS) found an asymptotically flat RBH which usually behaves like a Schwarzschild (SH) BH in Horava theory [14].

The pioneering work on accretion for spherical symmetry was by Bondi in the frame work of Newtonian gravity [15]. Many authors have investigated Bondi-type accretion flows in SH, SH de Sitter and SH anti-de Sitter BHs [16–18]. In this extension, Michel [19] proposed its general relativistic version by considering the steady state flow of a perfect fluid onto BH along the radial direction. The stability of Michel type accretion in the subsonic region has been analyzed by Moncrief [20]. Further, it was suggested by Babichev et al. [21] that the BH loses mass during the accretion of phantom dark energy onto it. Furthermore, many authors have worked on radial flows such as accretion of dark matter onto BHs [22] and radial accretion onto cosmological BHs [16,17], for self-gravitating [23,24] and perturbation theories [25]. The accretion onto an Einstein–Maxwell–Gauss–Bonnet BH and topologically charged BHs in $f(R)$ theories has been presented in [26,27]. The nonlinear study of a phantom scalar field accreted onto a BH was done by Gonzalez and Guzman [28] with the help of numerical methods. In this direction, some work has been done by various authors

[a] e-mails: jawadab181@yahoo.com; abduljawad@ciitlahore.edu.pk
[b] e-mail: m.u.shahzad@ucp.edu.pk

[2,29–31], and one showed that when phantom-like fluids accrete onto BHs/RBHs, then the mass of the BHs/RBHs decreases, respectively.

Recently, Chaverra et al. [1] and Ahmed et al. [32,33] have discussed Michel-type accretion near SH, and $f(R)$ and $f(T)$ BHs. In the present work, we will use a similar technique in order to discuss the accretion onto the well-known RBHs.The rest of the paper is organized as follows: in Sect. 2, we derive a general formalism for the spherically static accretion process. In Sect. 3, we discuss the accretion process using a Hamiltonian dynamical system and study the system at sonic points. In Sect. 4, we study two RBHs: KS-BH and RBH using the Dagum distribution function (DDF RBH). In Sect. 5, we find the solutions for isothermal test fluids of each RBH for different kinds of fluids. In Sect. 6, we investigate the accretion phenomena for a polytropic fluid. In the last section, we summarize our results.

2 General equations of spherical accretion

Here, we will derive the governing equations and analyze the flow of a perfect fluid and the accretion rate onto RBHs by utilizing the energy and particle conservation laws. In this way, we consider the general spherically symmetric set-up and the stationary line element is as follows:

$$ds^2 = -X(r)dt^2 + \frac{1}{X(r)}dr^2 + r^2(d\theta^2 + \sin^2\theta d\phi^2), \quad (1)$$

where $X(r) > 0$ is a function of r. The energy momentum tensor for a perfect fluid is given by

$$T_{\mu\nu} = (p + \varepsilon)u_\mu u_\nu + p g_{\mu\nu}, \quad (2)$$

where p is the pressure, ε is the energy density and u^μ is the four-velocity, which is given by

$$u^\mu = \frac{dx^\mu}{d\tau} = (u^t, u^r, 0, 0), \quad (3)$$

where τ is the proper time. Here, u^θ and u^ϕ become zero due to spherical symmetry restrictions. We define the current density or particle flux by $J^\mu = nu^\mu$. According to the law of particle conservation, the divergence of the particle flux is zero for this system, i.e.,

$$\nabla_\mu J^\mu = \nabla_\mu(nu^\mu) = 0, \quad (4)$$

where ∇_μ is the covariant derivative. It is useful to mention here that all the flow variables (p, ε, u^μ, n) are spherically symmetric and we have a steady state according to the definition of Michel [16,17]. Using Eq. (1) and the normalization condition $u^\mu u_\mu = -1$, we have

$$u_t = \pm\sqrt{u^2 + X(r)}, \quad (5)$$

where $u = dr/d\tau = u^r$, u^t can be negative or positive due to the square root which represents the backward or forward in time conditions. However, $u < 0$ is required for the accretion process, otherwise for any outward flows $u > 0$. The equation of continuity is

$$\nabla_\mu(nu^\mu) = \frac{1}{r^2}\partial_r(r^2 nu) = 0, \quad (6)$$

which leads to

$$r^2 nu = C_a, \quad (7)$$

where C_a is an integration constant. The thermodynamics of a perfect fluid is given by [34]

$$dp = n(dh - Tds), \quad d\varepsilon = hdn + nTds, \quad (8)$$

where $h = \frac{\varepsilon+p}{n}$ is the specific enthalpy, T is the temperature and s is the specific entropy.

Furthermore, the theorem of relativistic hydrodynamics (which is only applicable for smooth flows) states that the scalar quantities such as $hu_\mu\eta^\mu$ remain conserved along the trajectories of the fluid [34], i.e.,

$$u^\nu\partial_\mu(hu_\mu\eta^\mu) = 0, \quad (9)$$

where η^μ is a Killing vector of space-time. Considering $\eta^\mu = (1, 0, 0, 0)$ of the metric (1), we obtain

$$h\sqrt{u^2 + X(r)} = C_b, \quad (10)$$

where C_b is integration constant. It is also mentioned here that the specific entropy remains conserved along the fluid trajectories, i.e., $u^\mu\nabla_\mu s = 0$. Hence, the stress energy tensor $T_{\mu\nu}$ can be written as [32,33]

$$T_{\mu\nu} = nhu_\mu u_\nu + (nh - \varepsilon)g_{\mu\nu},$$

and then projection of $T^{\mu\nu}$ onto u^μ turns out to be

$$u_\nu\nabla_\mu T^{\mu\nu} = u_\nu\nabla_\mu[nhu_\mu u_\nu + (nh - \varepsilon)g_{\mu\nu}]$$
$$= -nTu^\mu\nabla_\mu s = 0. \quad (11)$$

Since the fluid is stationary (independent of time) and moving along the radial direction only in the present case, $\partial_r s = 0$ and hence s becomes constant. In this scenario, Eq. (8) reduces to

$$dp = ndh, \quad d\varepsilon = hdn. \quad (12)$$

Next, we will use Eqs. (7), (10) and (12) to analyze the flow. Since s becomes constant, the canonical form of the EoS of the simple fluid ($\varepsilon = \varepsilon(n, s)$) [32,33] turns out to be the barotropic form and is given by

$$\varepsilon = F(n). \quad (13)$$

In view of the above relation, Eq. (12) leads to

$$h = \frac{d\varepsilon}{dn} = \frac{dF(n)}{dn} = F'(n),$$
$$p' = nF'' \implies p = nF' - F, \tag{14}$$

which provides the relationship between F and G ($p = G(n)$) as follows:

$$G(n) = nF'(n) - F(n). \tag{15}$$

Further, the sound speed can be defined as $a^2 = (\partial p / \partial \varepsilon)_s$, which reduces to $a^2 = dp/d\varepsilon$ because s is constant. Using (12), we can find

$$\frac{dh}{h} = a^2 \frac{dn}{n}. \tag{16}$$

Using Eqs. (14) and (16), we obtain

$$a^2 = n(\ln F')'. \tag{17}$$

Since the motion is in the radial direction, the metric (1) reduces to

$$ds^2 = -(\sqrt{X(r)}dt)^2 + \left(\frac{dr}{\sqrt{X(r)}}\right)^2. \tag{18}$$

The ordinary three-velocity of the fluid can be defined as $v \equiv \frac{dr/\sqrt{X(r)}}{\sqrt{X(r)}dt}$ and its expression can be obtained by using the relations $u^t = dt/d\tau$, $u = u^r = dr/d\tau$, $u_t = -X(r)u^t$ and Eq. (5) as follows:

$$v^2 = \frac{u^2}{X(r) + u^2}, \tag{19}$$

which implies

$$u^2 = \frac{X(r)v^2}{1 - v^2} \quad \text{and} \quad (u_t)^2 = \frac{X^2(r)}{1 - v^2}. \tag{20}$$

Utilizing the above relations in (7), we obtain

$$C_a^2 = \frac{r^4 n^2 X(r) v^2}{1 - v^2}. \tag{21}$$

These results will be used in the following sections [32,33].

3 Hamiltonian system

Here, we derive two integrals of motion (C_a, C_b) given in (7) and (10) by adopting the Hamiltonian procedure. The idea of reformulating the Michel flow problem as a Hamiltonian system for global flow is analyzed in detail in [1,35–37]. The Hamiltonian H is a function of two variables (x, y) and its simplest form has one degree of freedom. Let H be the square of the LHS of Eq. (10):

$$H = h^2(X(r) + u^2). \tag{22}$$

Using Eq. (20) in the above equation, we have

$$H(r, v) = \frac{h(r, v)^2 X(r)}{1 - v^2}, \tag{23}$$

and this is derived in [32,33]. Here, we fixed the dynamical variables to be (r, v). For the derivation of critical points, particularly, the sonic points are derived in the following subsection.

3.1 Sonic points

The dynamical system of Hamiltonian H given in (23) reads [32,33]

$$\dot{v} = -H,_r, \quad \dot{r} = H,_v, \tag{24}$$

where a dot represents the derivative with respect to $\bar{t}$, which is a new "time" variable. The "time" variable $\bar{t}$ for the dynamical system is any variable on which Eq. (22) does not depend explicitly so that the dynamical system is autonomous. For finding critical points (CPs), we utilize Eq. (24) for which we require

$$\frac{d}{dr}H(r, v) = \frac{h^2}{1 - v^2}\left(\frac{d}{dr}(X(r)) + 2X(r)\frac{d}{dr}(\ln h)\right), \tag{25}$$

$$\frac{d}{dv}H(r, v) = \frac{2X(r)h^2 v}{(1 - v^2)^2}\left(1 + \frac{1 - v^2}{v^2}\frac{d}{dv}(\ln h)\right). \tag{26}$$

Moreover, Eq. (16) can be expressed as

$$\frac{d}{dr}(\ln h) = a^2 \frac{d}{dr}(\ln n), \tag{27}$$

$$\frac{d}{dv}(\ln h) = a^2 \frac{d}{dv}(\ln n). \tag{28}$$

By keeping r as a constant in Eq. (21), we have $\frac{nv}{\sqrt{1-v^2}} = $ constant, which by differentiation w.r.t. v leads to

$$\frac{d}{dv}(\ln n) = -\frac{1}{v(1 - v^2)} \Rightarrow \frac{d}{dv}(\ln h) = -\frac{a^2}{v(1 - v^2)}. \tag{29}$$

Similarly,

$$\frac{d}{dr}(\ln n) = -\frac{4 + r\frac{d}{dr}(\ln X(r))}{2r} \Rightarrow \frac{d}{dr}(\ln h)$$
$$= -\frac{a^2\left(4 + r\frac{d}{dr}(\ln X(r))\right)}{2r}. \tag{30}$$

Finally, by using Eqs. (24)–(30), we obtain

$$\dot{v} = -\frac{h^2}{r(1 - v^2)}\left(r\left(\frac{d}{dr}X(r)\right)(1 - a^2) - 4X(r)a^2\right), \tag{31}$$

$$\dot{r} = -\frac{2X(r)h^2}{v(1 - v^2)^2}\left(v^2 - a^2\right). \tag{32}$$

By setting the above relations equal to zero, we can get the CPs as follows:

$$v_c^2 = a_c^2 \quad \text{and} \quad r_c(1 - a_c^2)\frac{\mathrm{d}}{\mathrm{d}r_c}X(r_c) = 4X_c a_c^2. \tag{33}$$

Here $X_c \equiv X(r_c)$ and $\frac{\mathrm{d}}{\mathrm{d}r_c}X_c \equiv \frac{\mathrm{d}}{\mathrm{d}r}X(r) \mid_{r=r_c}$. The second relation of Eq. (33) represents the sound speed at the CP, i.e., a_c^2 in terms of r_c,

$$a_c^2 = \frac{r_c\frac{\mathrm{d}}{\mathrm{d}r_c}X_c}{4X_c + r_c\frac{\mathrm{d}}{\mathrm{d}r_c}X_c}. \tag{34}$$

In this scenario, the constant C_a^2 (21) can be written as

$$C_a^2 = r_c^4 n_c^2 v_c^2 \frac{X_c}{1 - v_c^2} = \frac{1}{4}r_c^5 n_c^2 \frac{\mathrm{d}}{\mathrm{d}r_c}X_c, \tag{35}$$

where we have used (33). Using C_a^2 in Eq. (21), we have

$$\left(\frac{n}{n_c}\right)^2 = \frac{r_c^5\left(\frac{\mathrm{d}}{\mathrm{d}r_c}X_c\right)(1 - v^2)}{4r^4 X(r)v^2}. \tag{36}$$

4 Regular black holes

In this section, we will discuss RBHs with fixed BH background, neglecting the self-gravity of the fluid.

4.1 KS regular black hole

Recently, Horava proposed the renormalizable gravity theory with higher order spatial derivatives in four dimensional space-time. It is an ultraviolet completion of general relativity. This theory reduces to Einstein gravity with non-vanishing cosmological constant in the infrared limit, but it has improved ultraviolet behaviors. Moreover, in deformed Horava–Lifshitz (HL) gravity, the ultraviolet properties are unchanged, whereas there exists a Minkowski vacuum in the infrared limit. The HL theory is considered as very interesting and many researchers discovered new BH solutions after its formulation [14,38–43]. Many new aspects are being discussed in connection with HL theory [44,45]. The metric function of KS RBH in deformed HL gravity is given by

$$X(r) = 1 + br^2\left(1 - \sqrt{1 + \frac{4M}{br^3}}\right), \tag{37}$$

where b is the arbitrary constant and M is BH mass. However, the constraints on the value of bM^2 have been developed through the comparison of perihelion shift test of KS BH with the observations in the solar system. It was found that $bM^2 \geq 1.7 \times 10^{-12}$ for Saturn, $bM^2 \geq 9 \times 10^{-12}$ for Mars and $bM^2 \geq 7.2 \times 10^{-10}$ for Mercury [46]. KS BH can be reduced to $X(r) = 1 - \frac{2M}{r} + \frac{2M^2}{br^4} + \cdots$ in the limiting case $b \to \infty$ or $r \to \infty$, while asymptotically it behaves as the

SH metric. The infrared properties of KS and RN BHs are different as shown in the third term of the expansion [47]. The KS metric has two horizons, r_h (outer) and r_{ch} (inner), and they can be obtained from the metric function (37) as follows:

$$r_{ch} = M\left(1 - \sqrt{\left(1 - \frac{1}{2bM^2}\right)}\right) \quad \text{and}$$

$$r_h = M\left(1 + \sqrt{\left(1 - \frac{1}{2bM^2}\right)}\right), \tag{38}$$

with $2bM^2 \geq 1$ [48]. For $2bM^2 = 1$, we have an extreme BH and for $2bM^2 < 1$, we have a naked singularity.

4.2 Regular black hole using Dagum distribution function

Consider the line element (1) for a generally spherically symmetric metric with

$$X(r) = 1 - \frac{2M}{r}\frac{\xi(r)}{\xi(\infty)}, \tag{39}$$

where the Dagum distribution function [49] is

$$\xi(x) = \frac{apx^{ap-1}}{b^{ap}\left(1 + \left(\frac{x}{b}\right)^a\right)^{p+1}}, \tag{40}$$

and a, b, p are positive parameters. By assuming $b = 1$ and $p = 1/a$, we find

$$\xi(x) = \frac{1}{\left(1 + x^a\right)^{\frac{a+1}{a}}}. \tag{41}$$

After replacing $x \to \frac{q^2}{Mr}$ and simplification leads to

$$X(r) = 1 - \frac{2M}{r}\left(\frac{1}{\left(1 + r\left(\frac{q^2}{Mr}\right)^a\right)^{\frac{a+1}{a}}}\right)^{\beta}. \tag{42}$$

This BH satisfies the weak energy condition for $\beta = \frac{3}{a+1}$ and hence we have

$$X(r) = 1 - \frac{2M}{r}\left(\frac{1}{1 + r\left(\frac{q^2}{Mr}\right)^a}\right)^{3/a}. \tag{43}$$

Moreover, one can find the RBH metric by using the Dagum distribution function with a factor q/r^2, which behaves asymptotically as an RN metric and its metric function is

$$X(r) = 1 - \frac{2M}{r}\left(\frac{1}{1 + \gamma\left(\frac{q^2}{Mr}\right)^a}\right)^{\frac{3}{a}} + \frac{q^2}{r^2}\left(\frac{1}{1 + \gamma\left(\frac{q^2}{Mr}\right)^a}\right)^{\frac{4}{a}}, \tag{44}$$

where $\gamma > 0$ is a constant and $a \geq 2$ is an integer. It should be noted that the associated solution satisfies the weak energy condition if we have $\gamma \geq (2/3)^a$, as shown in [50]. The associated electric field expression is given by

$$E = \frac{q}{r^2} \left(\frac{3\gamma(3+a)\left(\frac{q^2}{Mr}\right)^{a-1}}{2\left(1+\gamma\left(\frac{q^2}{Mr}\right)^a\right)^{2+\frac{3}{a}}} + \frac{1 - 3\gamma(3+a)\left(\frac{q^2}{Mr}\right)^a}{\left(1+\gamma\left(\frac{q^2}{Mr}\right)^a\right)^{2(2+a)/a}} \right). \tag{45}$$

The metric with function (44) behaves like the de Sitter BH metric as

$$X(r) \approx 1 - \frac{M^4}{\gamma^{\frac{4}{a}} q^6} (2\gamma^{\frac{1}{a}} - 1) r^2. \tag{46}$$

It can be noticed that the term proportional to r^2 cannot become zero because $\gamma \geq (2/3)^a$. The metric function (44) remains regular, if we set $(1/2)^a \leq \gamma < (2/3)^a$, but they have a de Sitter center without satisfying the weak energy condition. Therefore, if the BH metric is regular and satisfies the weak energy condition, then it has a de Sitter center [51]. However, if the metric has a de Sitter behavior when approaching the center, it does not necessarily satisfy the weak energy condition. Furthermore, if we set $\gamma < (1/2)^a$, the BH metric is not regular. Finally, there is a known case which can be obtained as a particular case of Eq. (44) by choosing $a = 2$ and $\gamma = \frac{M^2}{q^2}$, i.e.,

$$X(r) = 1 - \frac{2M\left(\frac{r^2}{r^2+q^2}\right)^{3/2}}{r} + \frac{q^2}{r^2}\left(\frac{r^2}{r^2+q^2}\right)^2. \tag{47}$$

This case corresponds to the RBH metric given in [52] and we will discuss the accretion onto this RBH in the following sections.

5 Isothermal test fluids

The fluid flowing at a constant temperature is known as an isothermal fluid. In the accretion process, the sound speed of the fluid flow remains constant. Moreover, the speed of sound at sonic points is equal to the speed of sound of accretion flow at any radius [32]. Here, we follow [33] to find the general solution of isothermal EoS of the form $p = k\varepsilon$, which leads to $p = kF(n)$ and $G(n) = kF(n)$ given in Eqs. (13) and (15), respectively, where k ($0 < k \leq 1$) is the state parameter. The differential equation (15) becomes

$$nF'(n) - F(n) = kF(n), \tag{48}$$

using (13) and integrating the above equation, we have

$$\varepsilon = F = \frac{\varepsilon_c}{n_c^{k+1}} n^{k+1}, \tag{49}$$

where $\frac{\varepsilon_c}{n_c^{k+1}}$ appears as an integration constant and hence Eq. (14) becomes

$$h = \frac{(k+1)\varepsilon_c}{n_c} \left(\frac{n}{n_c}\right)^k. \tag{50}$$

Using Eq. (36), we have

$$h^2 \propto \left(\frac{1 - v^2}{v^2 r^4 X(r)}\right)^k \tag{51}$$

and

$$H(r, v) = \frac{X^{1-k}(r)}{\left(1 - v^2\right)^{1-k} v^{2k} r^{4k}}, \tag{52}$$

where all constants get absorbed in the redefinition of the Hamiltonian H and the time $\bar{t}$. Next, we need to discuss the pressure physically. Using the EoS $p = k\epsilon$ and by substituting Eq. (36) in (49), we get

$$p \propto \left(\frac{1 - v^2}{X(r)v^2 r^4}\right)^{\frac{k+1}{2}}. \tag{53}$$

If this pressure approaches the event horizon from the region where t is time-like, then $X(r) \to 0$ and the speed $v \to 0$ or 1. In this situation, the Hamiltonian remains constant on the solution curve. For $v \to 0$, the solution curve approaches the horizon and hence the pressure diverges. For $v \to 1$, Eq. (53) remains finite in the surrounding of the horizon [32,33]. If $X(r) = 0$ has a single root as $r \to r_h$, then using (53) one can observe the pressure diverges as

$$p \sim \left(r - r_h\right)^{-\frac{k+1}{2k}}. \tag{54}$$

If $X(r) = 0$ has a double root then

$$p \sim \left(r - r_h\right)^{-\frac{k+1}{k}}. \tag{55}$$

The Hamiltonian (52) of the dynamical system is a constant along the solution curve. A global flow solution that extends to spatial infinity is

$$v \simeq v_1 r^{-\alpha} + v_\infty \quad as \ r \to \infty, \tag{56}$$

where ($v_1, |v_\infty| \leq 1, \alpha > 0$) are constants. Substituting Eq. (56) in Hamiltonian (52), we obtain

$$H \simeq \frac{X^{1-k}(r)}{r^{4k}} \quad 0 < |v_\infty| < 1, \tag{57}$$

$$H \simeq \frac{X^{1-k}(r)}{r^{(4-2\alpha)k}} \quad |v_\infty| = 0, \tag{58}$$

$$H \simeq \frac{X^{1-k}(r)}{r^{(4k+k\alpha-\alpha)}} \quad |v_\infty| = 1. \tag{59}$$

Now the behavior of the fluid is analyzed by considering different choices of the state parameter k such as $k = 1/4$ (sub-relativistic fluid), $k = 1/3$ (radiation fluid), $k = 1/2$
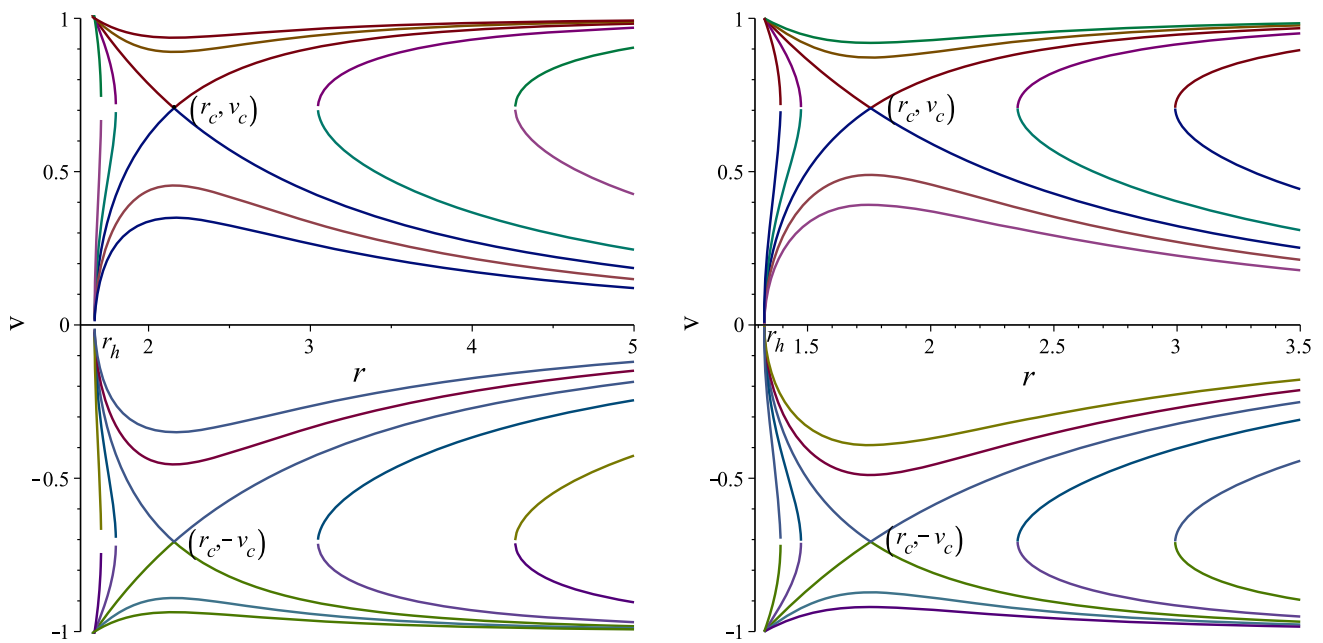
Fig. 1 Case $k = 1/2$. *Left panel* plot of (62) for KS BH with $M = 1$, $b = 0.9$. *Right panel* plot of (62) for the DDF RBH with $M = 1$, $q = 0.6$

(ultra-relativistic fluid) and $k = 1$ (ultra-stiff fluid), and these cases are discussed in the following subsections.

5.1 Solution for ultra-stiff fluid ($k = 1$)

We assume the fluids with EoS $p = \epsilon$ and these are ultra-stiff fluids. For instance, the usual EoS for the ultra-stiff fluids is $p = k\varepsilon$, i.e., the value of the state parameter is defined as $k = 1$. The Hamiltonian (52) reduces to

$$H = \frac{1}{v^2 r^4}. \tag{60}$$

In this case, the metric function $X(r)$ is not involved and it is discussed in detail in [1,32,33].

5.2 Solution for ultra-relativistic fluid ($k = 1/2$)

Here, we consider the fluids with EoS $p = \epsilon/2$ and these fluids are ultra-relativistic. The Hamiltonian takes the simple form

$$H = \frac{\sqrt{X(r)}}{r^2 |v| \sqrt{1 - v^2}}. \tag{61}$$

It is clear from this expression that the point $(r, v^2) = (r_h, 1)$ is not a critical point of the dynamical system. For some given value of $H = H_c$, Eq. (61) can be solved for v^2 as follows:

$$v^2 = \frac{1 \pm \sqrt{1 - 4f(r)}}{2} \tag{62}$$

where $f(r) \equiv \frac{X(r)}{H_c r^4}$. We plot the above velocity of the fluid (v) versus r for the aforementioned two RBHs such as KS

RBH and DDF RBH by inserting the corresponding values of $X(r)$ as shown in the left and right panels of Fig. 1, respectively. The trajectories in Fig. 1 correspond to values of $H_0 = \{H_c, H_c \pm 0.04, H_c \pm 0.09\}$ where $H = H_c = 0.170615$ (for KS RBH) and $H = H_c = 0.170615$ (for the DDF RBH). However, the values of (r_h, r_c, v_c) are approximately equal to $(1.66, 2.1575, 0.707107)$ and $(1.32, 1.75626, 0.707107)$ for KS RBH and DDF RBH, respectively. For $H = H_c = 0.170615$ (KS RBH) and $H = H_c = 0.232518$ (DDF RBH), the solution curves pass through the CPs $(r_c, -v_c)$ and (r_c, v_c). It is observed that the heteroclinic orbit exists in the range $-v_c < v < v_c$ and also passes through two CPs $(r_c, -v_c)$ and (r_c, v_c). It can also be seen that the fluid flow is closer to DDF RBH instead of KS BH. It is mentioned here that the fluid experiences the particle emission or fluid flow-out when $v > 0$, while the fluid accretes for $v < 0$. Moreover, Fig. 1 describes the following four types of fluid.

- We observe the supersonic/subsonic flows out of the fluid in the ranges $v_c < v < 1$ and $0 < v < v_c$, while subsonic/supersonic accretion appears in the ranges $-v_c < v < 0$ and $-1 < v < -v_c$, respectively.
- We have purely supersonic outflow for $v > v_c$ and purely supersonic accretion for $v < -v_c$.
- We have subsonic flow-out followed by subsonic accretion for $v_c > v > -v_c$.
- We have supersonic outflow followed by subsonic motion (upper plot) and subsonic accretion followed by supersonic accretion (lower plot).

According to the above discussion, we can say that the fluid outflow starts at the horizon because of its high pressure, which leads to divergence (can be seen from Eq. (54)) and the fluid under the effects of its own pressure flows back to spatial infinity [33]. From Fig. 1, we observe that the supersonic accretion is followed by subsonic accretion and ends inside the horizon, which does not give support to the claim that "the flow must be supersonic at the horizon" [53]. Thus, the flow of the fluid is neither transonic nor supersonic near the horizon [54,55]. These new solutions correspond to fine tuning and instability problems in dynamical systems. The issue of stability is related to the nature of saddle points (CPs (r_c, v_c) and $(r_c, -v_c)$) of the Hamiltonian function. Further analysis of stability could be done by using Lyapunov's theorem or a linearization of dynamical system [56–58] and their variations [59]. Another stability issue is the outflow of the fluid which starts in the surrounding of horizon under the effect of pressure being divergent. This outflow is unstable because it follows a subsonic path passing through the saddle point (r_c, v_c) and becomes supersonic with a speed approaching the speed of the light. The point $(r = r_h, v = 0)$ can be observed as attractor as well as repeller, where the solution curves converge and diverge, respectively, from the cosmological point of view [33,59].

5.3 Solutions for ($k = 1/3$) and ($k = 1/4$): Separatrix heteroclinic flows

The EoS with $k = 1/3$ and $k = 1/4$ describes the fluid such as a photon gas and sub-relativistic fluids (those fluids whose energy density exceeds their isotropic pressure), respectively. The Hamiltonian (52) for the above-mentioned fluids takes the following form:

$$H = \frac{X^{2/3}(r)}{r^{4/3}|v|^{2/3}(1-v^2)^{2/3}}, \qquad \text{for} \quad k = 1/3, \qquad (63)$$

$$H = \frac{X^{3/4}(r)}{r|v|^{1/2}(1-v^2)^{3/4}}, \qquad \text{for} \quad k = 1/4. \qquad (64)$$

It is clear from (63) and (64) that $(r, v^2) = (r_h, 1)$ are not CPs of the dynamical system. Figure 2 represents the contour plots of (63) and (64) in (r, v) for $k = 1/3$ (left panel) and $k = 1/4$ (right panel). We compare the fluid flow for the DDF RBH (red plot) and KS RBH (blue plot) in left panel ($k = 1/3$) and right panel ($k = 1/4$). For the case $k = 1/3$, there are two saddle points $(r_{c_1}, -v_{c_1})$ and (r_{c_1}, v_{c_1}) for DDF RBH and two saddle points $(r_{c_2}, -v_{c_2})$ and (r_{c_2}, v_{c_2}) for KS RBH. It is observed that the subsonic flow proceeds from the upper branch in lower plot, passes through CPs $(r_{c_1}, -v_{c_1})$ (DDF RBH) and $(r_{c_2}, -v_{c_2})$ (KS RBH), then crosses the hori-
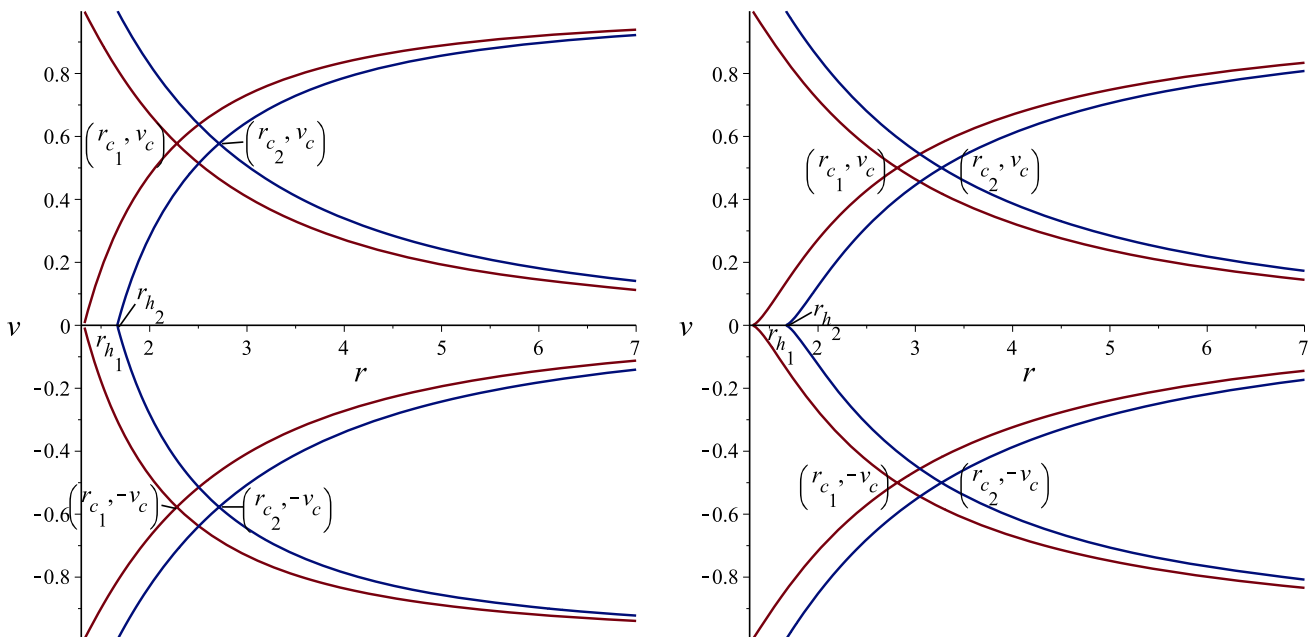

Fig. 2 *Left panel* case $k = 1/3$. Red plot of (63) for the DDF RBH with $q = 0.6$ and $M = 1$. The parameters are $r_h \simeq 1.33$, $r_{c_1} = 2.2787$ and $v_c = \frac{1}{\sqrt{3}} \simeq 0.57736$. The solution curve passes through the saddle CPs (r_{c_1}, v_c) and $(r_{c_1}, -v_c)$ for which $H = H_c \simeq 0.261266$. *Blue plot* of (63) for KS RBH with $b = 0.9$ and $M = 1$. The parameters are $r_h \simeq 1.68$, $r_{c_2} = 2.71329$ and $v_c = \frac{1}{\sqrt{3}} \simeq 0.57736$. The solution curve passes through the saddle CPs (r_{c_2}, v_c) and $(r_{c_2}, -v_c)$ for which

$H = H_c \simeq 0.22373$. *Right panel* case $k \leq 1/4$. Red plot of (64) for the DDF RBH with $q = 0.6$ and $M = 1$. The parameters are $r_h \simeq 1.367$, $r_{c_1} = 2.81368$ and $v_c = 0.5$. The solution curve passes through the saddle CPs (r_{c_1}, v_c) and $(r_{c_1}, -v_c)$ for which $H = H_c \simeq 0.29985$. *Blue plot* is for Eq. (64) for KS RBH with $b = 0.9$ and $M = 1$. The parameters are $r_h \simeq 1.717$, $r_{c_2} = 3.2682$ and $v_c = 0.5$. The solution curve passes through the saddle CPs (r_{c_2}, v_c) and $(r_{c_2}, -v_c)$ for which $H = H_c \simeq 0.273276$
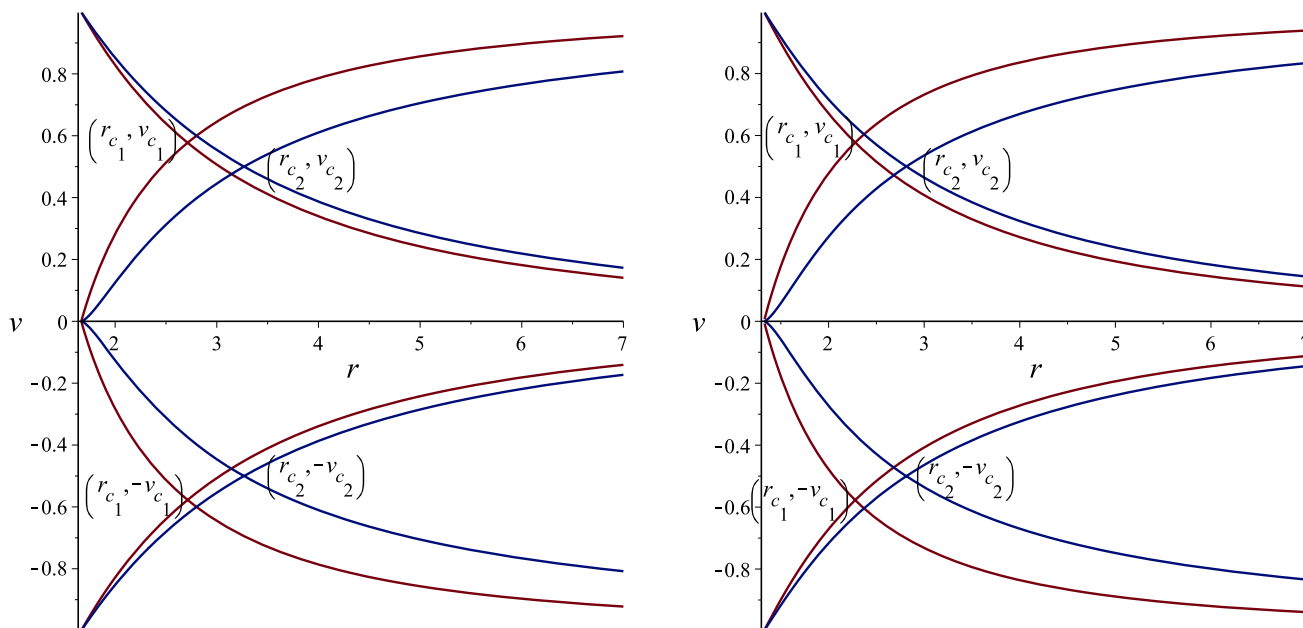
Fig. 3 Case $k \leq 1/3$. *Left panel*: red plot is for Eq. (63) for KS RBH with $b = 0.9$ and $M = 1$ ($k = 1/3$). The parameters are $r_h \simeq 1.717$, $r_{c_1} = 2.71329$ and $v_{c_1} = \frac{1}{\sqrt{3}} \simeq 0.57736$. *Blue plot* is for Eq. (64) for KS RBH $b = 0.9$ and $M = 1$ ($k = 1/4$). The parameters are $r_h \simeq 1.717$, $r_{c_2} = 3.2682$ and $v_{c_2} = 0.5$. *Right panel*: Red plot is for

Eq. (63) for the DDF RBH with $q = 0.6$ and $M = 1$ ($k = 1/3$). The parameters are $r_h \simeq 1.33$, $r_{c_1} = 2.2787$ and $v_{c_1} = \frac{1}{\sqrt{3}} \simeq 0.57736$. *Blue plot* is for Eq. (64) for the DDF RBH $b = 0.9$ and $M = 1$ ($k = 1/4$). The parameters are $r_h \simeq 1.33$, $r_{c_2} = 2.2787$ and $v_{c_2} = 0.5$

zon r_{h_1} (DDF RBH) and r_{h_2} (KS RBH). On the other hand, supersonic flows proceed from the lower branch in lower plot again passing through the CPs $(r_{c_1}, -v_{c_1})$ and $(r_{c_2}, -v_{c_2})$; as the fluid approaches the horizon, v vanishes. The supersonic accretion proceeds from the upper branch of upper plot and passes through CPs (r_{c_1}, v_{c_1}) (DDF RBH) and (r_{c_2}, v_{c_2}) (KS RBH) and so on. For subsonic accretion, the fluid proceeds from the lower branch of the upper plot and passes through CPs and crosses the horizons. A similar behavior of fluid could be observed for the case $k = 1/4$ in the right panel of Fig. 2.

The left panel of Fig. 3 represents the comparison of (63) ($k = 1/3$) and (64) ($k = 1/4$) for KS RBH. It can be seen that if the value of k increases, then the saddle points shifted towards the KS RBH. Also, the right panel of Fig. 3 represents the comparison of (63) ($k = 1/3$) and (64) ($k = 1/4$) for the DDF RBH. A similar behavior of CPs is observed for the DDF RBH.

6 Polytropic test fluids

The polytropic EoS is

$$p = G(n) = Kn^{\alpha}, \tag{65}$$

where K and α are constants. One can apply the constraint $\alpha > 1$ for ordinary matter. From Eqs. (15) and (65), one can easily construct the expression of the specific enthalpy:

$$h = m + \frac{K\alpha n^{\alpha-1}}{\alpha - 1}, \tag{66}$$

where m is the baryonic mass. Using the above equation and the three-dimensional speed of sound (17), we have

$$a^2 = \frac{(\alpha - 1)U}{m(\alpha - 1) + U}, \tag{67}$$

where ($U \equiv K\alpha n^{\alpha-1}$). Equations (66) and (67) leads to

$$h = m \frac{\alpha - 1}{\alpha - 1 - a^2}. \tag{68}$$

Furthermore, using (23) and (66), we have

$$h = m \left(1 + Q \left(\frac{1 - v^2}{r^4 X(r) v^2} \right)^{(\alpha-1)/2} \right), \tag{69}$$

where

$$Q \equiv \frac{K\alpha n_c^{\alpha-1}}{m(\alpha - 1)} \left(\frac{r_c^5 X(r_c)_{,r_c}}{4} \right)^{\left(\frac{\alpha-1}{2}\right)} = \text{constant}. \tag{70}$$

Inserting (69) into (23), the Hamiltonian system takes the following form:

$$H = \frac{X(r)}{1 - v^2} \left(1 + Q \left(\frac{1 - v^2}{r^4 X(r) v^2} \right)^{\left(\frac{\alpha-1}{2}\right)} \right)^2, \tag{71}$$

where m^2 has been absorbed into a redefinition of $(\bar{t}, H)$. It is observed that $\frac{dX(r)}{dr} > 0$ for all r which implies that $Q > 0$
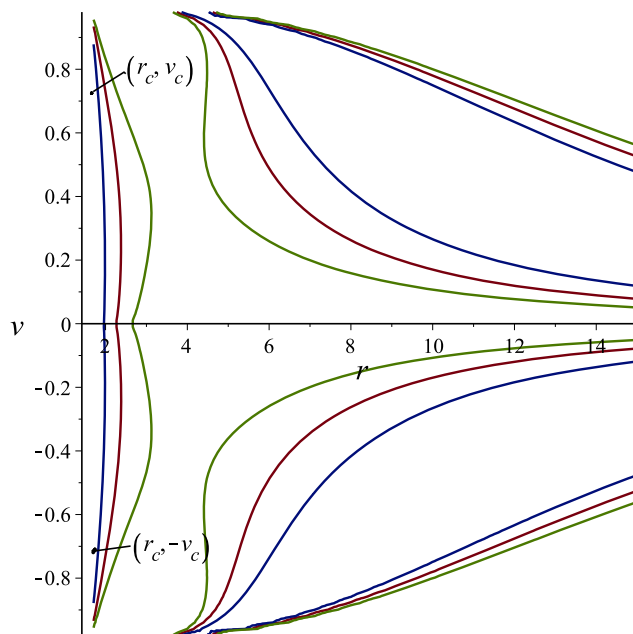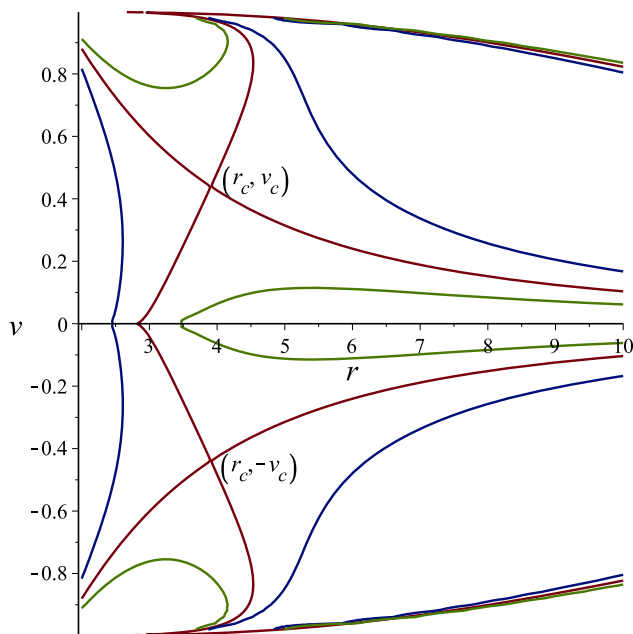
Fig. 4 *Left panel* contour plot of (71) for KS RBH with $b = 0.9$, $M = 1$, $\alpha = 0.5$, $Y = -1/8$ and $n_c = 0.19$. The parameters are $r_h \simeq 1.666666667$, $r_c \simeq 3.928297284$ and $v_c \simeq 0.4377733181$. The solution curve passing the CP (r_c, v_c) for $H = H_c \simeq 0.3173998409$. *Right* panel contour plot of (71) for DDF BH with $q = 0.5$, $M = 1$, $\alpha = 0.5$, $Y = -1/8$ and $n_c = 0.19$. The parameters are $r_h \simeq 1.614278177$, $r_c \simeq 1.988815258$ and $v_c \simeq 0.7359530796$. The solution curve avoiding the CP (r_c, v_c) for $H = H_c \simeq 0.2143193585$

with $\gamma > 1$. Hence, the square term in Eq. (71) is positive, while the coefficient $\frac{X(r)}{1-v^2}$ diverges as r approaches infinity ($0 \leq 1 - v^2 < 1$). Thus the Hamiltonian also diverges.

Using the technique of the authors of [32,33], we finally arrive at the following system:

$$(\alpha - 1 - v_c^2) \left(\frac{1 - v_c^2}{r_c^4 X(r_c) v_c^2} \right)^{(\alpha-1)/2} = \frac{n_c}{2Y} \left(r_c^5 X(r_c)_{r_c} \right)^{\frac{1}{2}} v_c^2,$$

(72)

$$v_c^2 = \frac{r_c X(r_c)_{r_c}}{r_c X(r_c)_{r_c} + 4X(r_c)}.$$

(73)

By plugging Eq. (73) in (72), we find r_c and then the corresponding v_c from (73). It is observed from Eq. (72) that $\alpha < 1$, $v_c^2 > \alpha - 1$ as mentioned in [32].

The left panel of Fig. 4 represents the contour plot of (71) for KS BH with $b = 0.9$, $M = 1$, $\alpha = 0.5095$, $Y = -1/8$ and $n_c = 0.19$. We find the new behavior of the fluid by finding the exact CP $r_c \simeq 3.928297284$, $v_c \simeq 0.4377733181$ for which $H = H_c \simeq 0.3173998409$. It can be observed that the accretion starts from subsonic flow for $r \to \infty$ and then follows supersonic passing through the saddle point and ends into the horizon. However, the supersonic flows out as observed in the vicinity of horizon passing through the saddle point and ends subsonically for $r \to \infty$. The right panel of Fig. 4 represents the contour plot of (71) for the DDF RBH

with $q = 0.5$, $M = 1$, $\alpha = 0.5$, $Y = -1/8$ and $n_c = 0.19$. We find the CP at $r_c \simeq 1.988815258$, $v_c \simeq 0.7359530796$ for which $H = H_c \simeq 0.2143193585$. We notice that the accretion starts from subsonic flow for $r \to \infty$ and then follows supersonically avoiding the saddle point and ends into the horizon. However, the supersonic outflow observed in the vicinity of horizon avoids the saddle point and ends subsonically for $r \to \infty$. These features agree with GR BHs [32,33].

In Fig. 5, we assume $\alpha = 1.9$, $Y = 1/8$, $n_c = 0.001$ in the left panel for KS RBH and $\alpha = 1.8$, $Y = 1/8$, $n_c = 0.001$ in the right panel for the DDF RBH, which leads to four CPs for each RBH, but none of them is a saddle point. There are three types of flow: (1) non-heteroclinic flow because the solution curves avoiding the CPs and accretion starting from the leftmost point until the horizon, (2) followed by non-relativistic outflow and (3) subsonic non-global flow. There are two other types of fluid flow: (1) partly subsonic accretion and flow-out with source-sink at the rightmost point of both graphs, and (2) partly supersonic accretion and flow-out with source-sink at the rightmost point of both graphs. Other solutions could also be found at $\alpha = 1.8$ for KS RBH and at $\alpha = 5.5/3$ for the DDF RBH. Since the fluid is considered as a test matter in the geometry of BH, we observe no homoclinic flow i.e. flow following a closed path [32,33].
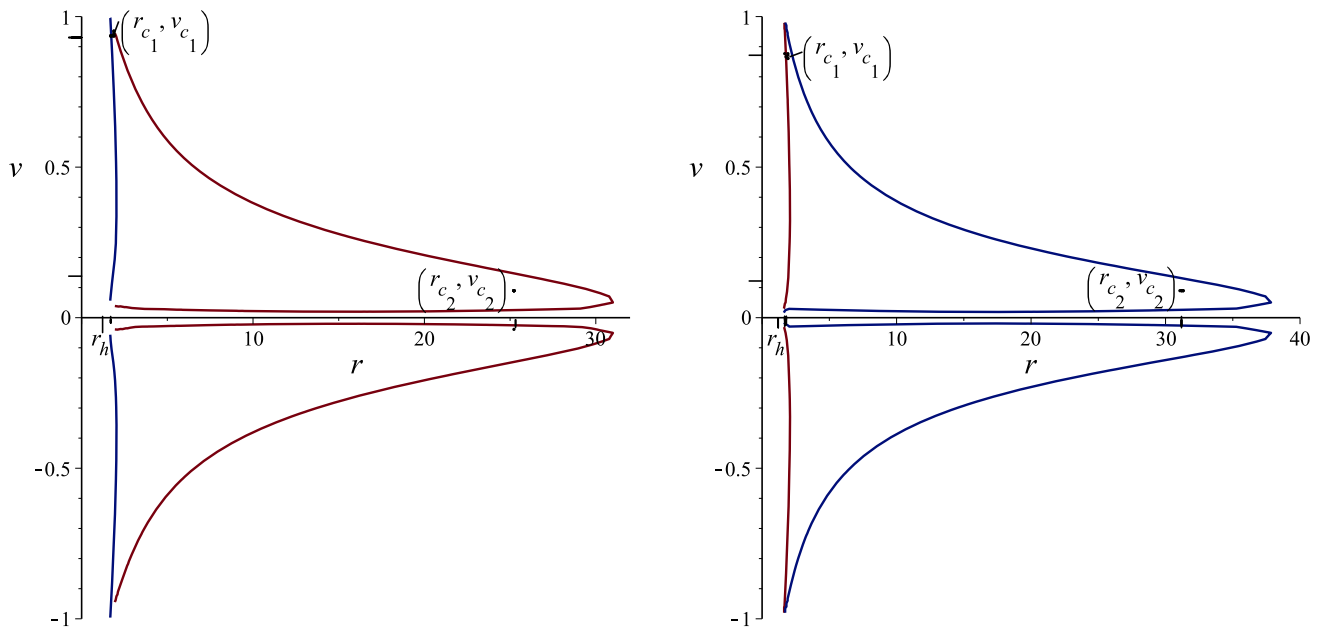
Fig. 5 *Left panel* contour plot of (71) for KS RBH with $b = 0.9$, $M = 1$, $\alpha = 1.9$, $Y = 1/8$ and $n_c = 0.001$. The parameters are $r_h \simeq 1.666666667$, $r_{c_1} \simeq 1.719016508$, $v_{c_1} \simeq 0.9439334159$, $r_{c_2} \simeq 25.49303509$ and $v_{c_2} \simeq 0.1443387155$. *Red plot* is the solution curve passing through (r_{c_2}, v_{c_2}) and $(r_{c_2}, -v_{c_2})$ with $H = H_{c_2} = 0.9452241039$. *Blue plot* is the solution curve passing through (r_{c_1}, v_{c_1}) and $(r_{c_1}, -v_{c_1})$ with $H = H_{c_2} = .2028972112$. *Right panel*

contour plot of (71) for DDF RBH with $q = 0.5$, $M = 1$, $\alpha = 1.8$, $Y = 1/8$ and $n_c = 0.001$. The parameters are $r_h \simeq 1.614278177$, $r_{c_1} \simeq 1.724674282$, $v_{c_1} \simeq 0.8893889966$, $r_{c_2} \simeq 31.59490067$ and $v_{c_2} \simeq 0.1283035425$. *Blue plot* is the solution curve passing through (r_{c_2}, v_{c_2}) and $(r_{c_2}, -v_{c_2})$ with $H = H_{c_2} = 0.9576657920$. *Red plot* is the solution curve passing through (r_{c_1}, v_{c_1}) and $(r_{c_1}, -v_{c_1})$ with $H = H_{c_2} = 0.2585395967$

7 Conclusion

In this work, we studied the steady state spherically symmetric accretion onto RBHs. Applying the technique of [32,33] and developing the Hamiltonian dynamical system we tackle the accretion problem. The pressure, baryon number density and other densities diverge on horizon, while the three-velocity has remained bounded by -1 and 1, and hence it does not diverge on the horizon. We have studied the motion of isothermal relativistic, ultra-relativistic, radiation and sub-relativistic test fluids in the frame work of Hamiltonian dynamical system around RBHs. The thermodynamical properties of fluids have been studied for different choices of EoS parameter. Moreover, CPs and conserved quantities have been found for different fluids. The behavior of an accreting fluid has been discussed as subsonic and supersonic according to EoS and RBHs. We compared the fluid flow for two different RBHs and observed that the fluid flow and CPs are closer to DDF RBH instead of KS RBH (Fig. 1). If CP is the saddle point, then the solution curve divides the (r, v) plane into the regions where fluid flow is physical for higher values of the Hamiltonian and unphysical in lower values of the Hamiltonian.

It has been observed that the supersonic accretion followed by subsonic accretion ends inside the horizon and it does not give support to the claim that "the flow must be

supersonic at the horizon" [53]. Hence the flow of the fluid is neither transonic nor supersonic near the horizon [54,55]. These new solutions correspond to fine tunning and instability problems in dynamical systems. Furthermore, we have observed from Fig. 3 that if the value of EoS parameter *(k)* increases, then the CPs shifted towards both RBHs. Hence, it is concluded that the three-velocity depends on CPs and the EoS parameter on phase space. It is interesting to mention here that the results obtained in Fig. 1 agree with [32,33]. We have also observed from the right panel of Fig. 4 that accretion starts from the subsonic case and ends at the supersonic case into the horizon, but avoiding the saddle points for the DDF RBH. Hence no saddle point occurs in the solution of the DDF RBH. Furthermore, the subsonic flow appears to be almost non-relativistic. These features agrees with GR BHs [32,33]. On the other hand, in the left panel of Fig. 4, it is seen that accretion starts from the subsonic case and ends in the supersonic case into the horizon but passing through the saddle points for KS RBH. Hence, the saddle point occurs in the solution of KS RBH. These features are different from [32,33].

References

1. E. Chaverra, O. Sarbach, Class. Quant. Grav. **32**, 15 (2015)
2. A. Jawad, M.U. Shahzad, Eur. Phys. J. C **76**, 123 (2016)
3. E. Elizalde, S.R. Hildebrandt, Phys. Rev. D **65**, 124024 (2002)
4. O.B. Zaslavskii, Phys. Lett. B **688**, 278 (2010)
5. S.W. Hawking, G.F. Ellis, *The Large Scale Structure of SpaceTime* (Cambridge Univ Press, Cambridge, 1973)
6. J.M.M. Senovilla, Gen. Relat. Gravit. **30**, 701 (1998)
7. J.M. Bardeen, in *Abstracts of the 5th International Conference on Gravitation and the Theory of Relativity*, ed. by V.A. Fock, et al. (Tbilisi University Press, Tbilisi, 1968), p. 174
8. E. Ayn-Beato, A. Garca, Phys. Rev. Lett. **80**, 5056 (1998)
9. A. Borde, Phys. Rev. D **50**, 3692 (1994)
10. A. Borde, Phys. Rev. D **55**, 7615 (1997)
11. S.A. Hayward, Phys. Rev. Lett. **96**, 031103 (2006)
12. W. Berej, J. Matyjasek, D. Tryniecki, M. Woronowicz, Gen. Relativ. Gravit. **38**(5), 885906 (2006)
13. B. Leonardo et al., Phys. Rev. D **90**, 124045 (2014)
14. A. Kehagias, K. Sfetsos, Phys. Lett. B **678**, 123 (2009)
15. H. Bondi, MNRAS **112**, 195 (1952)
16. J. Karkowski, E. Malec, Phys. Rev. D **87**, 044007 (2013)
17. P. Mach, E. Malec, Phys. Rev. D **88**, 084055 (2013)
18. P. Mach, E. Malec, J. Karkowski, Phys. Rev. D **88**, 084056 (2013)
19. F.C. Michel, Astrophys. Space Sci. **15**, 153 (1972)
20. V. Moncrief, Astrophys. J. **235**, 1038 (1980)
21. E. Babichev et al., Phys. Rev. Lett. **93**, 021102 (2004)
22. F.S. Guzman, F.D. Lora-Clavijo, MNRAS **415**, 225 (2011)
23. E. Malec, Phys. Rev. D **60**, 10403 (1999)
24. F.D. Lora-Clavijo, M. Gracia-Linares, F.S. Guzman, MNRAS **443**, 2242 (2014)
25. D.B. Ananda, S. Bhattacharya, T.K. Das, Gen. Relat. Gravit. **47**, 96 (2015)
26. C.S.J. Pun et al., Phys. Rev. D **78**, 024043 (2008)
27. S. Chakraborty, Class. Quant. Grav. **32**, 075007 (2015)
28. J.A. Gonzalez, F.S. Guzman, Phys. Rev. D **79**, 121501 (2009)
29. U. Debnath, Eur. Phys. J. C **75**, 129 (2015)
30. S. Bahamonde, M. Jamil, Eur. Phys. J. C **75**, 508 (2015)
31. M. Azreg-Aïnou, Eur. Phys. J. C **77**, 36 (2017)
32. Ahmed et al., Eur. Phys. J. C **76**, 269 (2016)
33. Ahmed et al., Eur. Phys. J. C **76**, 280 (2016)
34. L. Rezzolla, O. Zanotti, *Relativistic Hydrodynamics* (Oxford University Press, Oxford, 2013)
35. E. Chaverra, O. Sarbach, AIP Conf. Proc. **1473**, 54 (2011)
36. E. Chaverra, M.D. Morales, O. Sarbach, Phys. Rev. D **91**, 104012 (2015)
37. E. Chaverra, P. Mach, O. Sarbach, Class. Quant. Grav. **33**, 10 (2016)
38. Mu-In Park, JHEP **0909**, 123 (2009)
39. P. Horava, Phys. Lett. **B694**, 172 (2010)
40. P. Horava, JHEP **0903**, 020 (2009)
41. P. Horava, Phys. Rev. D **79**, 084008 (2009)
42. P. Horava, Phys. Rev. Lett. **102**, 161301 (2009)
43. T. Harko, Z. Kovacs, F.N. S. Lobo, Proc. R. Soc. Lond. A Math. Phys. Eng. Sci. (2010)
44. Y.S. Myung, Phys. Lett. **B685**, 318 (2010)
45. R. A. Konoplya, Phys. Lett. **B679**, 499 (2009)
46. L. Iorio, M.L. Ruggiero, Int. J. Mod. Phys. D **20**, 1079 (2011)
47. M. Eune, B. Gwak, W. Kim, Phys. Lett. B **718**, 1505 (2013)
48. H. Culetu, Astrophys. Space Sci. **2**, 360 (2015)
49. C. Dagun, Economie Appliquee. **30**, 413 (1977)
50. L. Balart, E. C. Vagenas, Phys. Rev. D **90**, 124045 (2014)
51. I. Dymnikova, Class. Quant. Grav. **19**, 725 (2002)
52. E. Ayon-Beato, A. Garcia, Phys. Rev. Lett. **80**, 5056 (1998)
53. S.K. Chakrabarti, Int. J. Mod. Phys. D **20**, 1723 (2011)
54. I. Novikov, K.S. Thorne, in *Black Holes*, ed. by C. DeWitt, B. DeWitt (Gordon and Breach, New York, 1973), p. 343
55. S.K. Chakrabarti, *Theory of Transonic Astrophysical Flows* (World Scientific, Singapore, 1990)
56. R.K. Nagle, E.B. Saff, A.D. Snider, *Fundamentals of differential equations and boundary value problems*, 6th edn. (Pearson, International Edition, UK, 2012)
57. J. Polking, A. Boggess, D. Arnold, *Diffrential Equations with Boundary Value Problems*, 2nd edn. (Prentice Hall, Upper Saddle River, 2006)
58. P. Bugl, *Differential Equations: Matrices and Models* (Prentice Hall, Englewood Cliffs, 1995)
59. M. Azreg-Anou, Class. Quantum Grav. **30**, 205001 (2013)